PCCP

Accepted Manuscript

ROYAL SOCIETY OF CHEMISTRY

www.rsc.org/pccp

Thermoelectric Performance of Ni compensated Cerium and Neodymium Double Filled *p*-type Skutterudites

Tulashi Dahal, Qing Jie, Yucheng Lan, Chuanfei Guo, and Zhifeng Ren*

Department of Physics and Texas Center for Superconductivity, University of Houston, Houston, TX 77204

*To whom correspondence should be addressed: zren@uh.edu

Abstract

We have synthesized Ni compensated Ce and Nd double filled *p*-type skutterudites $Ce_xNd_xFe_{3.7}Ni_{0.3}Sb_{12}$ with x = 0.35, 0.40, 0.45, and 0.5 by melting-quenching-annealing method. The samples were made by directly hot pressing the hand ground powder at 650 ^oC for 5 minutes at a pressure of about 80 MPa. Since Ni has two more electrons than Fe, a lower power factor and stronger bipolar effect in thermal conductivity are expected at higher temperature. In the experiments, we have demonstrated that by suitably tuning Fe-Ni ratio and filler concentration, we can achieve both a higher power factor (~35 μW cm^{-1} K^{-2} at 535 ^oC) and a lower thermal conductivity (~2.1 W m^{-1} K^{-1} at room temperature and ~2.7 W m^{-1} K^{-1} at 535 ^oC) in $Ce_{0.4}Nd_{0.4}Fe_{3.7}Ni_{0.3}Sb_{12}$. A peak thermoelectric figure-of-merit of ~1.1 at 475 ^oC was achieved in $Ce_{0.4}Nd_{0.4}Fe_{3.7}Ni_{0.3}Sb_{12}$.

Introduction

In the industrial process, about 60% of the total heat is wasted. By using thermoelectric (TE) materials, we may capture a fraction of the waste heat and convert it into useful electric power [1]. The ability of a TE material to convert heat into electricity is quantified by a dimensionless thermoelectric figure-of-merit, *ZT*, defined as $ZT = \frac{S^2\sigma}{\kappa}T$, where S is the Seebeck coefficient, σ is the electrical conductivity, κ is the thermal conductivity ($\kappa = \kappa_e + \kappa_l$, where κ_e and κ_l are carrier and lattice contribution, respectively), and *T* is the absolute temperature. A good thermoelectric material should have high electrical conductivity, high Seebeck coefficient and a low thermal conductivity. But, the interdependency between these transport properties makes the optimization of *ZT* extremely challenging.

The phonon glass electron crystal, called "PGEC" is believed to have electron transport just like in crystalline solid while thermal transport like that in glass [2]. Skutterudite compounds are viewed as one class of PGEC materials [3]. Recently, skutterudite compounds have attracted an increased attention due to its reasonable band gap, higher carrier mobility [4], lower cost and environmentally friendly constituents compared to other thermoelectric materials. Since the crystal structure of skutterudite is cubic, there is no need to worry about the anisotropy on the electrical and thermal transport properties, which make them easy for assembling into devices without worrying the orientation.

Skutterudites compounds are of the form RM_4X_{12} in which there are voids that can be filled with element *R*, called guest atom or filler or rattler in literature (we use rattler in this paper), may be alkali metal [5, 6], alkaline-earth metal [7, 8], rare earth or actinide [9, 10], *M* is transition metal (Co, Rh, or Ir) and *X* is the pnictogen atom (P, As, or Sb). Rattlers in the skutterudite void plays two important roles: first, it donates the carriers to the host compound to tune the electrical property; secondly, the Einstein-like vibration of rattlers in the void behaves as phonon scattering center and substantially reduces lattice thermal conductivity [11, 12]. The vibrational frequencies of rattler species are specific to their atomic mass and are different for different elements [13, 14, 15, 16]. Generally, rattlers with smaller ionic radii, which are loosely bounded with Sb ring, rattle with higher amplitude and frequency of vibration, and enhance the phonon scattering to significantly reduce the lattice thermal conductivity [17]. Thus, filling the

voids by multiple rattlers with different atomic masses and radii has been proved to be an effective way to scatter a broad range of phonons, which significantly reduces the lattice thermal conductivity leading to improved *ZT* [18, 19, 20]. Elemental substitution method in Sb ring is also proven to be an effective way to reduce the lattice thermal conductivity by phonon scattering via mass fluctuation leading to higher *ZT* [21], comparable to single filled skutterudites [22].

The peak *ZT* of *p*-type skutterudites [23, 24, 25] is lower compared to *n*-type skutterudites [18, 19]. Therefore, improving thermoelectric performance of *p*-type RFe_4Sb_{12} compounds is desired.

Most of the previously reported work in *p*-type skutterudites involves a partial replacement of Fe by Co [23, 26, 27, 28]. Recently, Cho *et al.* reported a peak *ZT* ~0.9 at 740 K for $Yb_{0.95}Fe_{3.5}Pt_{0.5}Sb_{12}$ made by hot pressing the ground powder at 903 K under a pressure of 50 MPa [29]. Zhou *et al.* synthesized Yb/La double filled *p*-type skutterudites and reported a peak *ZT* ~1 at 700 K in $Yb_{0.25}La_{0.60}Fe_{2.7}Co_{1.3}Sb_{12}$ [28]. Tan *et al.* synthesized Ce filled *p*-type skutterudites with excess Ce using melt spinner followed by Spark Plasma Sintering (SPS) and reported a peak *ZT* ~1 at about 800 K in $Ce_{1.1}Fe_4Sb_{12}$ [30]. Zhang *et al.* synthesized Nd filled *p*-type skutterudites replacing Sb partially by Ge and reported the presence of nano-particle of the size less than 100 nm covered by film-like features in the matrix of $Nd_{0.6}Fe_2Co_2Sb_{11.7}Ge_{0.3}$, reducing the thermal conductivity leading to a peak *ZT* ~1.1 at 700 K [25]. Jie *et al.* reported fast phase formation in double filled *p*-type skutterudites $Ce_{0.45}Nd_{0.45}Fe_{3.5}Co_{0.5}Sb_{12}$ and reported a power factor of ~36 $\mu W\ cm^{-1}\ K^{-2}$, leading to a peak *ZT* ~1.1 at around 750 K [24]. For device performance, higher power factor is desired to maximize power output [31] since higher power factor with a higher thermal conductivity generates more power than the lower power factor with lower thermal conductivity even though they have similar *ZTs*.

In literature, there are few reports on *p*-type skutterudites in which Fe is replaced by Ni [32, 33]. In this paper, we reported a systematic study of Ni substitution in the thermoelectric properties of *p*-type skutterudites. We first kept the concentration of rattlers, *x* fixed at $x = 0.45$ and tuned Fe/Ni ratio to study the effect of Ni substitution on thermoelectric properties. Subsequently, we chose the best Fe/Ni ratio that yielded the highest *ZT* and tuned the rattlers

concentration. By this method, we demonstrated that a suitable ratio of Fe/Ni together with an appropriate amount of rattlers would result in a power factor ~35 μW cm^{-1} K^{-2} leading to a peak *ZT* ~1.1 at 475 ^{o}C. Considering the recent work from Jie *et al.,* [24], the sample synthesized in this work has similar power factor and *ZT* value. However, we have a smaller amount of rattlers and Co is replaced by a smaller amount of cheaper element Ni, which could be cost effective when considering the bulk production for practical applications.

Experiment

Stoichiometric amount of elements (Ce ingot (99.8%, Alfa Aesar), Nd ingot (99.6%, Alfa Aesar), Fe pieces (99.999%, Alfa Aesar), Ni slugs (99.98% Alfa Aesar), and Sb Chunk (99.999%, Chengdu Chemphys Chemical Industry, China) were weighed and kept in carbon coated quartz tube inside a glove box. The tubes were sealed at a low pressure of the order of 2×10^{-6} mbar, kept in furnace, melted at 1080 ^{0}C for 24 hours, and quenched in cold water. The produced ingots were then annealed at 650 ^{0}C for 5 days to ensure the pure skutterudite phase. The ingots were then taken out of the tubes, cleaned using a steel brush and ultra-sonication in ethanol. The dried ingots were then hand ground to fine powder using mortar and pestle in an argon protected environment. The ground powder was then hot pressed in a graphite die at 650 ^{0}C with a pressure of about 80 MPa for 5 minutes to get a sample disk of about 4 mm thickness. The disks were cut into two half-disks of about 2 mm thick each. One of them was polished to get a uniform thickness for thermal diffusivity measurement (LFA 454, Netzsch) while the other disk was used to make a $2\times2\times12$ mm^3 bar for electrical conductivity and Seebeck coefficient (ZEM-3, Ulvac) measurements. We paid particular attention to the sample uniformity and found that the properties of these two disks are similar and there is no anisotropy. The density of all samples was measured using Archimedes' kit and the heat capacity was measured using DSC (DSC 404 C, Netzsch). The total thermal conductivity was then calculated as $\kappa = \alpha C_p \rho$, where α is the thermal diffusivity, C_p is the heat capacity at constant pressure, and ρ is the density of the sample.

The phase formation of the samples was characterized by X-ray diffraction on an X'pert PRO PANalytical diffractometer with Cu Kα radiation source. The microstructure of the

samples was studied by scanning electron microscopy (SEM) (LEO 1500, JEOL) and transmission electron microscopy (TEM) (JEM-2100F, JEOL). The hot pressed samples were cut into blocks (2 mm by 3mm by 1 mm) and mechanically polished. The polished specimen was glued on a copper grid and then Ar-ion milled to an electron transparent specimen on a Precision Ion Polishing System (Gatan Inc.). The energy of Ar-ions was 3.5 keV and its incident angle was 3.5^{o}. The chemical composition of hot pressed samples was analyzed by energy dispersive X-ray diffractometer (JSM 6330F, EDAX). The error in the measurement of Sb and Fe is less than 5%, while it is about 10% for Ce, Nd, and Ni measurement.

Results and discussion

Fig. 1 shows the XRD patterns of four compositions studied. The XRD patterns of the hot pressed samples show pure skutterudites phase without any impurity phase for x = 0.35, 0.40, and 0.45 indicating that the structure is flexible to accommodate different amount of rattlers. However, we observed impurity phase for the sample with x = 0.5.

Fig. 2 shows the SEM image at low (Fig. 2a) and high (Fig. 2b) magnification of the freshly broken surface of the hot pressed samples. From the SEM images, we have observed that the majority of the grains are of micron size and only a few grains are of nano-scale size. With the bigger grains, we have few interfaces for phonon scattering. But, the non-uniform distribution of grain size can help scatter phonons with different mean free paths [34] even though it may not be as effective as what was shown in reference [34]. The SEM image shows that the crystallized grains are closed packed, an indication of high volume mass density. The measured densities of 7.72, 7.70, 7.78, and 7.82 g cm^{-3} for x = 0.35, 0.40, 0.45, and 0.5, respectively of the sample are more than 97% of the theoretical density, which is consistent with close packing shown in the SEM images. The high resolution TEM image in Fig. 2c shows that the grain boundaries are clean and the orientations are of large angles, which also helps phonon scattering.

Table 1 shows the compositions studied, their actual compositions, and various properties at room temperature.

Fig. 3a shows the temperature dependent electrical conductivity of samples. The electrical conductivity of all samples decrease with temperature, showing that all samples are heavily doped semiconductors. We also observed that the electrical conductivity of the samples with higher rattler concentration is lower. In the experiments we have kept the Fe to Ni ratio fixed, the electrical conductivity of the samples depends on the filler concentration. Higher Ce and Nd contents give more electrons to skutterudite structure, effectively reducing the hole concentration which, in turn, reduces the electrical conductivity, which is consistent with the observed electrical conductivity.

The temperature dependent Seebeck coefficient is shown in Fig. 3b. The Seebeck coefficient of all samples is positive, implying that the dominant charge carriers are holes, and is consistent with the electrical conductivity measurement. For a given temperature difference, high Seebeck voltage is required to convert a significant fraction of heat into useful electricity. We have achieved a high Seebeck voltage of ~173 μV K^{-1} at around 535 ^{o}C in $Ce_{0.40}Nd_{0.40}Fe_{3.7}Ni_{0.3}Sb_{12}$, the composition with the highest *ZT* in this experiment. From the temperature dependent Seebeck coefficient measurement, the band gap (E_g) of various compositions can be roughly estimated using the equation $E_g = 2eS_{max}T_{max}$, where e is the elementary charge, S_{max} is the peak Seebeck coefficient, and T_{max} is the maximum temperature corresponding to the maximum Seebeck coefficient [35]. Based on this equation, the band gaps of samples were estimated to be in the range of 0.25-0.29 eV, consistent with literature value [36].

The temperature dependent power factor is shown in Fig. 3c. The power factor, *PF*, of all samples increases with temperature and attains a maximum value at around 530 ^{o}C. A maximum power factor of ~35 μW cm^{-1} K^{-2} at around 535 ^{o}C is achieved in $Ce_{0.4}Nd_{0.4}Fe_{3.7}Ni_{0.3}Sb_{12}$, and is comparable to some of the *p*-type compositions reported previously [24, 33].

The temperature dependent thermal conductivity is shown in Fig. 3d. The thermal diffusivity of the samples as a function of temperature is shown in the inset of Fig. 3d. The total thermal conductivity for $Ce_xNd_xFe_{3.7}Ni_{0.3}Sb_{12}$ with x = 0.40, 0.45, and 0.5 is lower than that of $Ce_{0.35}Nd_{0.35}Fe_{3.7}Ni_{0.3}Sb_{12}$. For $Ce_{0.35}Nd_{0.35}Fe_{3.7}Ni_{0.3}Sb_{12}$, the total thermal conductivity increases with temperature. This may be due to increased carrier contribution to the total thermal

conductivity and at the same time fewer rattlers will result in higher lattice thermal conductivity. For all of the samples, we observed an upturn in thermal conductivity after 325 ^{o}C. The observed upturn in thermal conductivity at higher temperature is due to the excitation of both electrons and holes across the gap, a well-known bipolar effect. Assuming that the contribution of minority charge carriers at high temperature is small, the total thermal conductivity can be written as the sum of the thermal contribution from the carriers and from the lattice vibration. The carrier contribution to the total thermal conductivity can be calculated using Wiedemann-Franz relation given by $\kappa_e = \sigma LT$, where σ is the electrical conductivity, L is the Lorenz number, and T is the absolute temperature. The Lorenz number can be calculated as [37]

$$L = \left(\frac{\kappa_B}{e}\right)^2 \left[\frac{\left(r+\frac{7}{2}\right)F_{r+\frac{5}{2}}(\xi)}{\left(r+\frac{3}{2}\right)F_{r+\frac{1}{2}}(\xi)} - \left(\frac{\left(r+\frac{5}{2}\right)F_{r+\frac{3}{2}}(\xi)}{\left(r+\frac{3}{2}\right)F_{r+\frac{1}{2}}(\xi)}\right)^2\right] \quad (1)$$

where r is the scattering parameter, and $F_n(\xi)$ is the Fermi integral given by,

$$F_n(\xi) = \int_0^\infty \frac{y^n}{1+e^{y-\xi}}dx \quad (2)$$

where ξ is the reduced Fermi energy that can be deduced from the Seebeck coefficient S as well as the scattering parameter r, given as

$$S = \pm\frac{\kappa_B}{e}\frac{\left(r+\frac{5}{2}\right)F_{r+\frac{3}{2}}(\xi)}{\left(r+\frac{3}{2}\right)F_{r+\frac{1}{2}}(\xi)} - \xi \quad (3)$$

In this calculation, we assumed that the acoustic phonon scattering is the dominant mechanism for carrier scattering and evaluated the temperature dependent Lorenz number from the reduced Fermi energy deduced from the Seebeck coefficient at room temperature based on single parabolic band model [38]. The lattice part of thermal conductivity can be inferred by subtracting the carrier contribution from the total thermal conductivity. The temperature dependent lattice thermal conductivity is shown in Fig. 3e. κ_l for most of the samples decreases with temperature and attains a minimum value at around 475 ^{o}C and then increases. For $Ce_{0.5}Nd_{0.5}Fe_{3.7}Ni_{0.3}Sb_{12}$, we observed an upturn in lattice thermal conductivity after 425 ^{o}C. The

lattice thermal conductivity of the sample with x = 0.35 is higher than that of sample with x = 0.40, which can be attributed to the weaker rattling effect due to lower filler concentration. For the sample with x = 0.45 and 0.50, the lattice thermal conductivity is higher than the sample with x = 0.35 and 0.40, possibly due to weaker rattling effect because of higher Ce and Nd concentration above the solubility limit [14, 39]. Among the four samples measured, the lattice thermal conductivity of $Ce_{0.4}Nd_{0.4}Fe_{3.7}Ni_{0.3}Sb_{12}$ is the lowest and varies from ~1.05 W m^{-1} K^{-1} at room temperature to ~0.8 W m^{-1} K^{-1} at 535 ^{o}C.

The temperature dependent ZT is calculated from the measured value of temperature dependent electrical conductivity (σ), the Seebeck coefficient (S), and the thermal conductivity (κ), and is plotted in Fig. 3f. The ZT value of all samples increases with temperature, attain a maximum value at around 475 ^{o}C, and then decreases. The peak ZT of ~1.1 at 475 ^{o}C in $Ce_{0.4}Nd_{0.4}Fe_{3.7}Ni_{0.3}Sb_{12}$ is comparable to the highest reported ZT of p-type skutterudites.

Conclusion

Ni-doped p-type skutterudites $Ce_xNd_xFe_{3.7}Ni_{0.3}Sb_{12}$ were synthesized by melting-quenching-annealing method followed by hot pressing the hand ground powder. The electrical conductivity decreased with increasing the Ce and Nd concentration, while the Seebeck coefficient increased. By tuning the Ce and Nd concentration, we achieved a low thermal conductivity of ~2.1 W m^{-1} K^{-1} at room temperature and ~2.7 W m^{-1} K^{-1} at 535 ^{o}C, and a power factor of ~35 μW cm^{-1} K^{-2} at around 535 ^{o}C in $Ce_{0.4}Nd_{0.4}Fe_{3.7}Ni_{0.3}Sb_{12}$. A peak ZT of ~1.1 was achieved in $Ce_{0.4}Nd_{0.4}Fe_{3.7}Ni_{0.3}Sb_{12}$.

Acknowledgement

This work is supported by DOE EERE SETP CSP program with the award number DEEE0005806.

References

1. L. E. Bell, *Science,* 2008, **321**, 1457.
2. G. A. Slack, *in CRC Handbook of Thermoelectrics*, Ed. M. Rowe (CRC Press, Boca Raton, FL, 1995) P. 407.
3. G. S. Nolas, G A Slack, S. B. Schujman, T. M Tritt (Ed.), *Semiconductors and Semimetals 69,* Academic Press, (2001).
4. C. Uher and T. M. Tritt, *In Recent Trends in Thermoelectric Matrials Research II, Semiconductors and semimetals,* Academic Press: San Diego, 2000, **69**, 139.
5. Y. Z. Pei, L. D. Chen, W. Zhang, X. Shi, S. Q. Bai, X. Y. Zhao, Z. G. Mei, and X. Y. Li, *Appl. Phys. Lett.,*2006, **89**, 221107.
6. Y. Z. Pei, J. Yang, L. D. Chen, W. Zhang, J. R. Salvador, and J. H. Yang, *Appl. Phys. Lett,* 2009,. **95**, 042101.
7. L. D. Chen, T. Kawahara, X. F. Tang, T. Goto, T. Hirai, J. S. Dyck, W. Chen, and C. Uher, *J. Appl. Phys*., 2001, **90**, 1864 .
8. X. Y. Zhao, X. Shi, L. D. Chen, W. Q. Zhang, W. B. Zhang, and Y. Z. Pei, *J. Appl. Phys.,*2006, **99**, 053711.
9. V. L. Kuznetsov, L. A. Kuznetsova, and D. M. Rowe, *J. Phys.: Condens. Matter*, 2003, **15**, 5035.
10. G. A. Lamberton, S. Bhattacharya, R. T. Littleton, M. A. Kaeser, R. H. Tedstrom, T. M. Tritt, J. Yang, and G. S. Nolas, *Appl. Phys. Lett.,* 2002, **80**, 598.
11. B. C. Sales, D. Mandrus, and R. K.Williams, *Science*, 1996, **272**, 1325.
12. D. J. Singh and M. H. Du, *Phys. Rev. B,* 2010, **82**, 075115.
13. M. V. Keepens, D. Mandrus, B. C. Sales, B. C. Chakoumakos, P. Day, R. Coldea, B. Maple, D. A. Gajewski, E. J. Freeman, and S. Bennington, *Nature (London), 1998,* **395**, 876.
14. L. Zhang, A. Grytsiv, P. Rogl, E. Bauer, and M. Zehebauer, *J. Phys. D: Appl. Phys*., 2009, **42**, 225405.
15. J. Yang, W. Zhang, Z. Q. Bai, Z. Mei, and L. D. Chen, *Appl. Phys. Lett*., 2007, **90**, 192111.
16. X. F. Tang, Q. Zhang, L. D. Chen, T. Goto, and T. Hirai, *J. Appl. Phys.,* 2005, **97**, 093712.

17. X. Shi, S. Q. Bai, L. Xi, J. Yang, W. Q. Zhang, L. Chen, and J. H. Yang, J. Mater. Res., 2011, **15**, 1745.
18. X. Shi, J. Yang, J. R. Salvador, M. F. Chi, J. Y. Cho, H. Wang, S. Q. Bai, J. H. Wang, W. Q. Zhang, and L.D. Chen, *J. Am. Chem. Soc* 2011, **133**, 7837.
19. X. Shi, H. Kong, C. P. Li, C. Uher, J. Yang, J. R. Salvador, H. Wang, L. Chen, and W. Zhang, *Appl. Phys. Lett.,* 2008, **92**, 182101.
20. W. Zhao, P. Wei, Q. Zhang, C. Dong, L. Liu, and X. F. Tang, *J. Am. Chem. Soc.,* 2009, **131**, 3713.
21. X. Su, H. Li, G. Wang, H. Chi, X. Y. Zhou, X. F. Tang, Q. Zhang, and C. Uher, *Chemistry of Materials*, 2011, **23**, 2948.
22. J. Yang, Q. Hao, H. Wang, Y. C. Lan, Q. Y. He, A. Minnich, D. Z. Wang, J. A. Harrisman, V. M. Varki, M. S. Dresselhaus, G. Chen, Z. F. Ren, *Phys. Rev. B*, 2009, **80**, 115329.
23. H. Li, X. Tang, Q. Zhang, and C. Uher, *Appl. Phys. Lett.,* 2009, **94**, 102114.
24. Q. Jie, H. Wang, W.S. Liu, H. Wang, G. Chen, and Z. F. Ren, *Phys. Chem. Chem. Phys*., 2013, **15**, 6809.
25. L. Zhang, F. Duan, X. Li, X. Yan, W. Hu, L. Wang, Z. Lu, Y. Tian, and B. Xu, *J. Appl. Phys,* 2013, **114**, 083715.
26. P. F. Qiu, J. Yang, R.H. Liu, X. Shi, X. Y. Huang, G. J. Synder, W. Zhang, and L. D. Chen, *J. Appl. Phys.*, 2011, **109**, 063713.
27. G. Rogl, A. Grytsiv, P. Rogl, E. Bauer, M. B. Kerber, M. Zehetbauer, and S. Puchegger, *Intermetallics*, 2010, **18**, 2435.
28. L. Zhou, P. Qiu, C. Uher, X. Shi, and L.Chen, *Intermetallics,* 2013, **32**, 209-213.
29. J. Y. Cho, Z. Ye, M. M. Tessema, J. R. Salvador, R. A. Waldo, *J. Appl. Phys*., 2013, 113, 143708.
30. G. J. Tan, Y. Zheng, and X. F. Tan, *Appl. Phys. Lett*., 2013, **103**, 183904.
31. G. J. Snyder and T. S. Ursell, *Phys. Rev. Lett*., 2003, **91**,148301.
32. P. F. Qiu, R. H. Liu, J. Yang, X. Shi, X. Y. Huang, W. Zhang, L. D. Chen, J. Yang, and D. J. Singh, *J. Appl. Phys.,* 2012, **111**, 023705.
33. G. Rogl, A. Grystiv, P. Rogl, E. Royanian, E. Bauer, J. Horky, D. Setman, E. Schafler, and M. Zehetbauer, *Acta Materialia*, 2013, **61**, 6778.

34. K. Biswas, J. He, I. D. Blum, C. I. Wu, T. P. Hogan, D. N. Seidman, V. P. Dravid, and M. G. Kanatzidis, *Nature*, 2012, **489**, 414.
35. H. J. Goldsmith and J. W. Sharp, *J. Elec. Mater*., 1999, **28**, 869.
36. D. Mandrus, A. Miglori, T. W. Darling, M. F. Hundley, E. J. Peterson, and J. D. Thompson, *Phy. Rev. B,* 1995, **52**, 4926.
37. D. M. Rowe and C. M Bhandari, *Modern Thermoelectrics*, Reston Publishing, Reston, VA (1983).
38. W. S. Liu, Q. Y. Zhang, Y. C. Lan, S. Chen, X. Yan, Q. Zhang, H. Wang, D. Z. Wang, G. Chen, and Z. F. Ren, *Adv. Eng. Mater.,* 2011, **1**, 577-587.
39. D. T. Morelli, G. P. Meisner, B. X Chen, S. Q. Hu, and C. Uher, *Phys. Rev. B*, 1997, **56**, 7376.

Table 1: Room temperature thermoelectric properties of $Ce_xNd_xFe_{3.7}Ni_{0.3}Sb_{12}$ with x = 0.35, 0.40, 0.45, and 0.50 and their actual composition.

Nominal composition	Actual composition	Density ($g\ cm^{-3}$)	Electrical conductivity ($10^5\ S\ m^{-1}$)	Seebeck Coefficient ($\mu V\ K^{-1}$)	Thermal conductivity ($W\ m^{-1}\ K^{-1}$)	*ZT*
$Ce_{0.35}Nd_{0.35}Fe_{3.7}Ni_{0.3}Sb_{12}$	$Ce_{0.33}Nd_{0.29}Fe_{3.77}Ni_{0.29}Sb_{11.84}$	7.72	1.97	97	2.28	0.25
$Ce_{0.40}Nd_{0.40}Fe_{3.7}Ni_{0.3}Sb_{12}$	$Ce_{0.38}Ce_{0.37}Fe_{3.78}Ni_{0.27}Sb_{11.68}$	7.70	1.76	103	2.10	0.27
$Ce_{0.45}Nd_{0.45}Fe_{3.7}Ni_{0.3}Sb_{12}$	$Ce_{0.40}Nd_{0.36}Fe_{3.72}Ni_{0.32}Sb_{11.88}$	7.78	1.53	100	2.25	0.21
$Ce_{0.50}Nd_{0.50}Fe_{3.7}Ni_{0.3}Sb_{12}$	$Ce_{0.43}Nd_{0.41}Fe_{3.74}Ni_{0.28}Sb_{11.72}$	7.82	1.37	104	2.34	0.19

Figure Captions

Fig. 1. XRD patterns of hot pressed skutterudites $Ce_xNd_xFe_{3.7}Ni_{0.3}Sb_{12}$ samples with x = 0.35, 0.40, 0.45, and 0. 5. The sample with x = 0.50 shows impurity phase.

Fig. 2. SEM images at (a) low, (b) high magnification of $Ce_{0.40}Nd_{0.40}Fe_{3.7}Ni_{0.3}Sb_{12}$ samples showing the grain sizes, and (c) high resolution TEM image showing clean grain boundary and large orientation angle between grains.

Fig. 3. Temperature dependent thermoelectric properties of $Ce_{0.40}Nd_{0.40}Fe_{3.7}Ni_{0.3}Sb_{12}$ (x = 0.35, 0.40, 0.45, and 0. 5) samples: (a) electrical conductivity, (b) Seebeck coefficient, (c) power factor, (d) thermal conductivity, (e) lattice thermal conductivity, and (f) figure of merit, *ZT*.

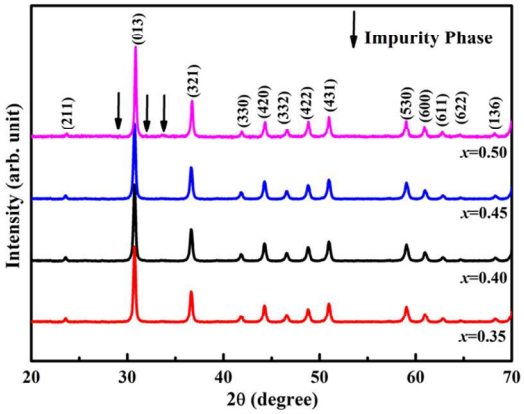

Fig. 1, T. Dahal *et al*

Fig. 1. XRD patterns of hot pressed skutterudites CexNdxFe3.7Ni0.3Sb12 samples with x = 0.35, 0.40, 0.45, and 0. 5. The sample with x = 0.50 shows impurity phase.
338x190mm (96 x 96 DPI)

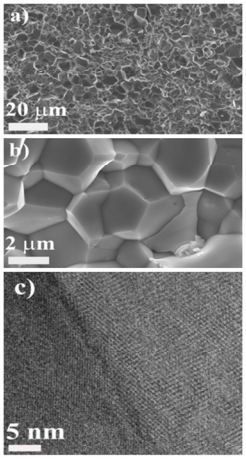

Fig. 2, T. Dahal *et al*

SEM images at (a) low, (b) high magnification of Ce0.40Nd0.40Fe3.7Ni0.3Sb12 samples showing the grain sizes, and (c) high resolution TEM image showing clean grain boundary and large orientation angle between grains.
338x190mm (96 x 96 DPI)

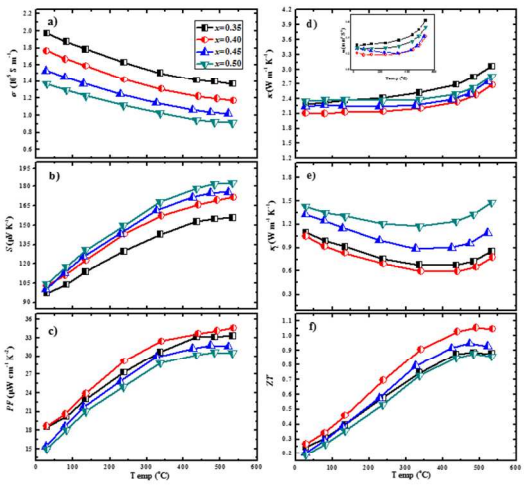

Fig. 3, T. Dahal *et al*

Temperature dependent thermoelectric properties of Ce0.40Nd0.40Fe3.7Ni0.3Sb12 (x = 0.35, 0.40, 0.45, and 0. 5) samples: (a) electrical conductivity, (b) Seebeck coefficient, (c) power factor, (d) thermal conductivity, (e) lattice thermal conductivity, and (f) figure of merit, ZT.
338x190mm (96 x 96 DPI)